FUEL

the science and technology of Fuel and Energy

Published by Butterworths

like exinites, resinites, alignites and scleronites might well disintegrate. Shibaoka[20] performed hot stage microscopy studies on vitrite particles (containing vitrinite >95%) and found that these expanded rapidly and then shrank without disintegrating. Fusinite particles, containing fusinite macerals >95%, were found in the same study to expand very slightly and not explode. The petrographic analysis of the two coals (*Table 5*) indicates that these coals have only small proportions of exinite material and hence most of the particles are not expected to explode. Shibaoka also found that vitrite particles leave behind very fine ash particles. However this would not be expected if the coal particle has an ash composition such that the ash would melt. Such ash particles would be mobile on the carbon surface in view of the non-wetting characteristics of slag on a carbonaceous surface[21], with agglomeration leading to a droplet of ash.

Recently Padia[22] has claimed that about five ash particles per coal particle are formed on combustion of bituminous coal. His analysis implied that the distribution of mineral matter was uniform in the coal particles, which the present study indicates is not valid, e.g., *Table 10* shows that ≈25% of the particles by weight had mineral matter varying from 5 to 100%. In the absence of definitive experiments, it is assumed that one coal particle produces one ash particle or that if more than one ash particle is formed from one coal particle, the composition of each satellite ash particle is the same. The major uncertainty in the use of the data was in construing the various types which might or might not lead to slag deposit. A more detailed understanding of the mechanism of slag deposit formation would enable a better choice of the important types: the data output of the computer can be readily manipulated to assign particles to types providing the characteristics of 'bad-acting' types were better understood.

ACKNOWLEDGEMENTS

The authors thank Mr Richard Borio and Mr Armand A. Levasseur of Combustion Engineering for supplying the coal samples and information regarding their behaviour in coal combustion. They thank Mr N. Suhr of The Pennsylvania State University for performing some of the coal analyses. This work was funded by the US Department of Energy under Contract EF-76-S-01-2316.

REFERENCES

1 Reid, W. T. 'External Corrosion and Deposits in Boilers and Gas Turbines', Elsevier Publishing Co., New York, 1971
2 Watt, J. D. and Fereday, F. *J. Inst. Fuel* 1969, **42**, 99
3 Watt, J. D. and Fereday, F. *J. Inst. Fuel* 1969, **42**, 131
4 Sage, W. L. and McIlroy, J. B. *J. Eng. Power* 1960, **82**, 145
5 Hoy, H. R., Roberts, A. G. and Wilkins, D. M. *Inst. Gas Eng. Comm.* 1964, 672
6 Corey, R. C. *US Bur. Mines Bull.* 1974, **618**, 64
7 Attig, R. C. and Duzy, A. F., 'Coal ash deposition studies and application to boiler design', Am. Power Conference, 22 April, 1969
8 Babcock and Wilcox Co., 'Guide specifications, cyclone furnace fuel system, coal', 7 February 1971
9 ASME Research Committee on Corrosion and Deposits from Combustion Gases report on 'Coal Fouling and Slagging Parameters', (Ed. R. C. Winegartner), 1974
10 Reid, W. T. and Cohen, P. *Furn. Perf. Factors Suppl. to Trans. ASME* 1944, **66**, 83
11 Troutman, S., Johnson, G. G. Jr., White, E. W. and Lebiedzik, J., American Laboratory, 1974, Feb., p. 31
12 Moza, A. K., Austin, L. G. and Johnson, G. G. Jr., SEM/1979/1, p. 473, SEM Inc. AMF O'Hare, IL 60666, USA
13 Moza, A. K., *Ph.D. Thesis*, Fuel Science, 1980
14 Moza, A. K., Strickler, D. W. and Austin, L. G., SEM/1978/I, p. 289, SEM Inc., AMF O'Hare, IL 60666, USA
15 Phase Diagrams for Ceramists, 3rd ed., (Eds. Levin, E. M. Robbins, C. R. and McMurdie, H. F.) Am. Ceramic Soc., 1964, Fig. 630
16 Phase Diagrams for Ceramists, 3rd ed., (Eds. Levin, E. M., Robbins, C. R. and McMurdie, H. F.) Am. Ceramic Soc., 1964, Figure 656 and 627
17 Moza, A. K., Austin, L. G. and Tressler, R. W., ASME paper no. 79-WA/FU-3
18 Raask, E. *Fuel* 1969, **48**, 366
19 Ramsden, A. R. *J. Inst. Fuel* 1969, **48**, 121
20 Shibaoka, M. *J. Inst. Fuel* 1969, **42**, 59
21 Raask, E., ASME paper No. 65-WA/FU-1
22 Padia, A. K. *D.Sc. Thesis*, Chem. Eng., MIT, Cambridge, USA, 1976

Physical characterization and pressure–temperature microscopy of the pyrite–pyrrhotite transformation

J. M. Lambert, Jr.*†, P. L. Walker, Jr.*, A. J. Perrotta, J. P. McCullough** and H. Beuther****

**Department of Materials Science and Engineering, Pennsylvania State University, University Park, PA 16802, USA*

***Gulf Research & Development Company, PO Drawer 2038, Pittsburgh, PA 15230, USA*

(Received 4 June 1982)

Structural changes occurring during the hydrogen-assisted pyrite–pyrrhotite transition are characterized over the temperature range 400–600°C. Newly developed pressure–temperature microscopy gave *in-situ* observations of pyrite decomposition at elevated temperatures and gas pressures. Composition of pyrrhotites was measured by X-ray diffraction and correlated with krypton surface areas. Surface areas increased with an increase in pyrite reduction due to a decrease in molar volume accompanied by the development of porosity. Increases in specific surface area are inversely proportional to the reduction temperature. Heats of adsorption of krypton on pyrite increase linearly with increases in the relative amount of the (100) crystallographic faces.

(Keywords: pyrite; pyrrhotite; microscopy; physical characterization)

The utilization of pyrite-containing coals in pyrolysis, gasification, or liquefaction processes at elevated temperatures and pressures results in the formation of pyrrhotite. *In-situ* coal conversion catalysis by mineral matter in coal, with special regard to the relatively more abundant pyrite constituent, has been recognized for some time[1–4]. More recently, hydrogen sulphide has been considered to be the catalytic species with increased hydrogen sulphide concentrations being initially supplied by pyrite reduction[5]. Study of the pyrite–pyrrhotite transition, during benzothiophene hydrogenolysis at coal liquefaction conditions, showed that the surface area of the resulting pyrrhotite increased with increasing pyrite particle size; however true areas were occluded by carbon deposits[6]. The purpose of this investigation is to characterize the pyrite–pyrrhotite transition without the presence of hydrocarbons that lead to catalytic coking and carbon deposition. The present study gives the changes in specific surface areas and porosity upon pyrite reduction in hydrogen, the composition of the pyrrhotites, the heats of adsorption of krypton on pyrite, and direct microscopic observations of the pyrite–pyrrhotite transition at elevated temperatures and pressures.

EXPERIMENTAL

Pyrite from Sonora, Mexico, was obtained from Ward's Natural Science Establishment. The pyrite was ground in a ceramic ball mill and wet-sieved into 210×250 and 44×53 μm particle-size fractions. The washing was performed using 2 N HCl to remove surface oxides and wash away alumino-silicate fines remaining from the ball mill. The two sized fractions were analysed for impurities by emission spectroscopy and found to be identical. Trace amounts (< 100 ppm) of cobalt and copper were only detected. X-ray analysis gave sharp, narrow peaks indicative of a crystallite size > 100 nm.

Pyrite samples of ≈ 2 g were placed in a ceramic boat which was inserted into a preheated tube furnace for reduction in flowing hydrogen (300 cm^3 min^{-1}, 0.1 MPa). The tube furnace was contained in a nitrogen-purged glovebox. Reductions of the 210×250 μm size particles were performed at 400, 450, 500, and 600°C. The smaller particle size, due to limited quantities, was reduced at 450 and 600°C. All temperatures were controlled to within ± 8°C of the desired reaction temperature. Fresh samples were reduced for various periods of time, then removed from the furnace and allowed to cool at room temperature in the nitrogen atmosphere. The composition and specific surface area of the products at various extents of conversion were then measured.

The surface areas of the samples were measured by a multipoint BET method[7] employing krypton at −196°C ($P_0 = 373$ Pa) as the adsorbate. Due to the small specific surface areas encountered (< 1 m^2 g^{-1}), the use of nitrogen at 0.1 MPa pressure was not sufficiently accurate. The pressure range of interest for krypton adsorption lies between 20 and 270 Pa. These pressures could be measured on a McLeod Gauge, but only at the expense of greatly increasing the system dead-space and loss of sensitivity. To circumvent this, a thermistor was placed into the volumetric adsorption apparatus, as shown in *Figure 1*. The thermistor was connected as one leg of a Wheatstone bridge through which a fixed current was passed. This caused the thermistor to heat to a particular temperature, and thus assume a fixed resistance. While under vacuum, the bridge was adjusted such that the null meter, N, read zero. As increasing pressures of krypton impinged on the thermistor, more heat was removed, lowering its temperature, and increasing its resistance.

* Present address: Standard Oil Company Research & Development, 9101 E. Pleasant Valley Road, Independence, OH 44131, USA

0016-2361/83/121474-07$3.00

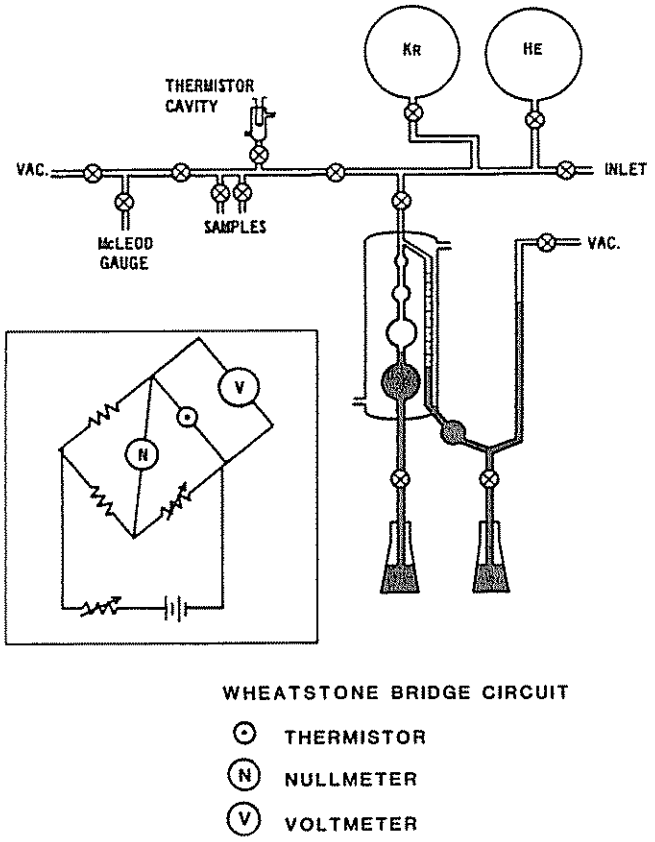

Figure 1 Krypton adsorption apparatus

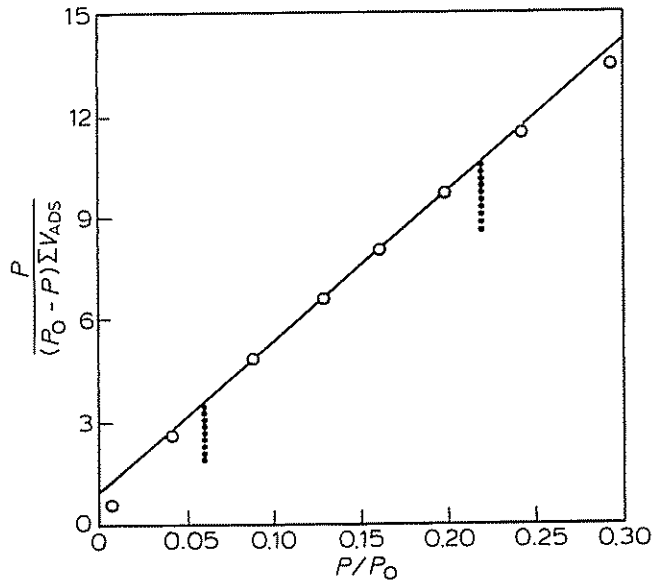

Figure 2 Typical BET plot. Linear region: $0.06 < P/P_o < 0.22$

The change in voltage-drop, V, across the thermistor was calibrated to pressure with the McLeod gauge. Once a calibration curve was obtained, the McLeod gauge was isolated from the system to maintain a small, constant dead-space. The volume of the dead-space was determined by expanding helium into the gas burette. Prior to measuring the surface area and system dead-space, all samples were outgassed overnight at 77°C. Additional details of the apparatus modifications and design can be found elsewhere[8].

A typical BET plot is shown in *Figure 2* for the adsorption of krypton on pyrrhotite. The reciprocal of the sum of the intercept and slope of a line drawn through the linear region of the plot ($0.06 < P/P_0 < 0.22$) yields the volume of the adsorbed monolayer. By assuming each adsorbed krypton molecule occupies 1.95×10^{-19} m^2 (reference 9), the surface area of the adsorbent can be calculated. The specific surface area is obtained by dividing this area by the sample weight.

The compositions of the pyrrhotite products were determined by the X-ray diffraction technique of Yund and Hall[10]. Cu-K_α radiation and CaF_2 internal standard were employed. This technique was chosen for compositional analysis because, as previously described[11], it permitted evaluation of the composition existing in the outermost layer of the particles. Particularly at low extents of conversion, a pyrite core may still exist within each particle; however, it is the degree of reduction of the pyrrhotite, located on the outside of the particle, which brings about the observed changes in surface area.

Microscopic observations on pyrite reduction were carried out in a newly developed pressure–temperature cell adapted to a Leitz hot stage. The pressure–temperature cell has a pressure range up to 14 MPa (2000 psi) and a temperature range of 0–600°C, while maintaining a continuous flow of gas over the sample. A picture of the cell as it is seated on the Leitz heating stage can be seen in *Figure 3*. The cell, shown in *Figure 4*, consists of a stainless steel body comprised of a lower and upper portion. The lower portion, which contains the

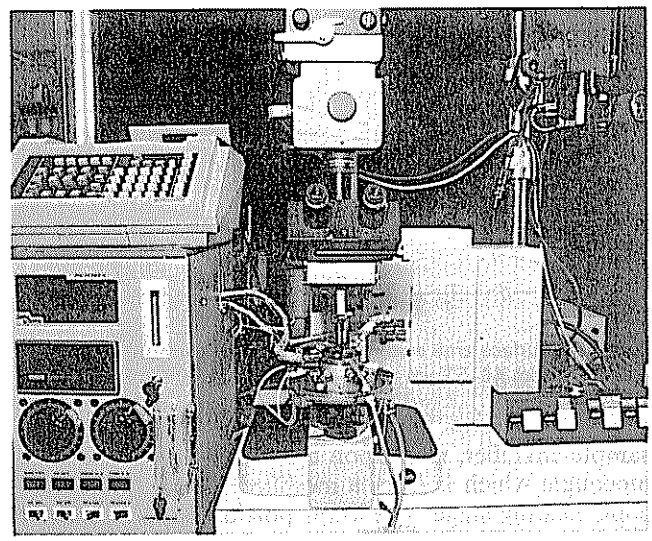

Figure 3 Pressure–temperature cell seated on Leitz 1350 hot stage

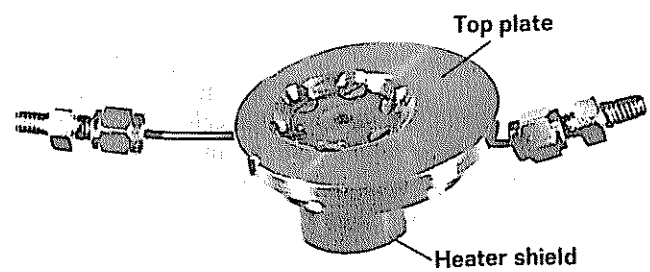

Figure 4 Gas flow pressure–temperature cell

Table 1 Surface areas of Sonora pyrite

Particle size (μm)	Specific surface area ($m^2\ g^{-1}$)		
	Measured	Sphere	R_f
210–250	0.017	0.0026	6.5
44–53	0.027	0.012	2.2

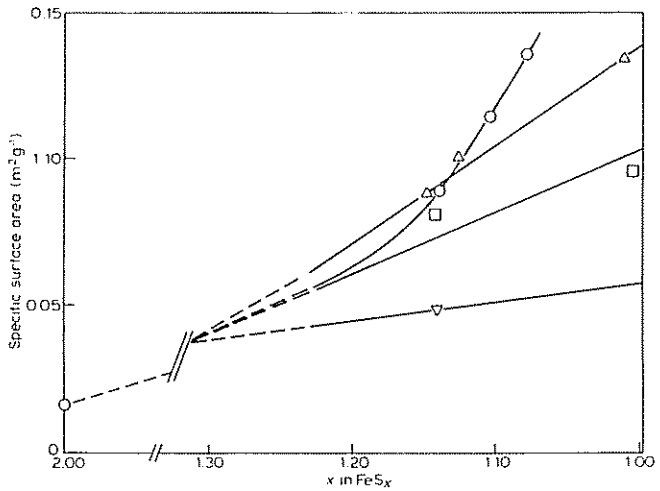

Figure 5 Surface area *versus* composition of pyrrhotites produced from 210–250 μm pyrite particles. ○, 400°C; △, 450°C; □, 500°C; ▽, 600°C

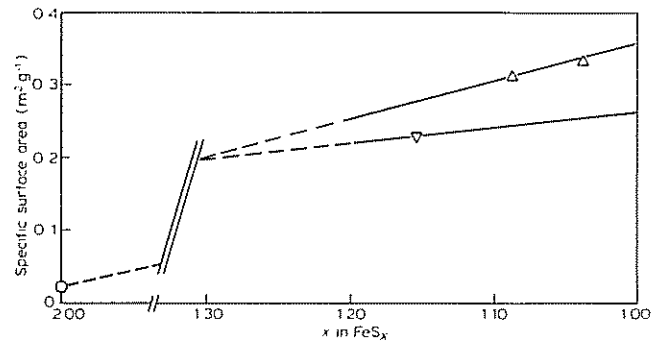

Figure 6 Surface area *versus* composition of pyrrhotites produced from 44–53 μm pyrite particles. △, 450°C; ▽, 600°C

sample chamber, rests upon a ceramic heater and thermocouple which is from a modified Leitz 1350 microscopic heating stage. The lower portion also contains an inlet and an outlet for flow of pressurized hydrogen gas. The flow rate can be as high as 4 $cm^3\ min^{-1}$ which is equivalent to 280 cell volumes/min. The sealing and viewing of the sample chamber is through a single crystal of spinel or yttrium-aluminium garnet resting on a specially designed copper o-ring which allowed for observations at elevated pressures and temperatures. The top portion of the cell both seals the sample chamber through six screws which are located away from the sample chamber, and sets the position of the cell on the microscope stage. The microscopic system can be programmed to desired heating or cooling rates. Volatiles and gases are analysed by a Hewlett Packard 5880 gas chromatograph after pressure reduction. Observations are made with a Leitz Orthoplan polarizing microscope and are recorded either with a 35 mm camera with automatic exposure control or a 16 mm OptiQuip Model 220 cinemicrography system incorporating automatically coupled film speed and exposure control during operation. A 450 W xenon lamp allows the highest shutter speeds possible using cross-polarized light.

RESULTS AND DISCUSSION

The surface area for the two size fractions of Sonora pyrite along with the geometric area calculated by assuming spheres with diameters of 230 and 48.5 μm are given in *Table 1*. Calculated roughness factors, R_f, are the ratios of the measured to calculated areas. The decrease in the roughness factor, with decreasing particle size, is most likely due to preferred cleavage during grinding. Preferred (100) cleavage in pyrite has been reported previously[12]. Smooth cleavage at a crystallographic face would yield a lesser degree of surface roughness than random fracturing of the particle.

The specific surface areas as a function of pyrrhotite composition for the 210–250 and the 44–53 μm pyrite are shown in *Figures 5* and *6*, respectively. The surface areas increase with the extent of conversion of pyrite to pyrrhotite. Pyrrhotite compositions with sulphur contents $> FeS_{1.15}$ were not obtained in agreement with accepted phase equilibria[11]. The maximum increase in specific surface area is ≈ 10-fold; this is considerably less than the area increases previously reported where simultaneous carbon deposition had occurred[6].

The increase in specific surface area with extent of reduction is shown to be inversely proportional to temperature, suggestive of sintering. Photomicrographs were taken by scanning electron microscopy of the four samples shown in *Figure 5* having a composition of $\approx FeS_{1.14}$. The photomicrographs (*Figure 7*) show the particle size essentially unchanged; the direct microscopic study, to be discussed later, further supports these observations. The increase in surface area is attributed to the development of porosity and additional internal surfaces. The visible difference in the porosity between *Figures 7a* and *7b* is minimal, coinciding with the nearly equal surface areas given in *Figure 5*. *Figures 7c* and *7d* show decreasing porosity with increasing temperature of reduction. The specific surface areas of these samples, as

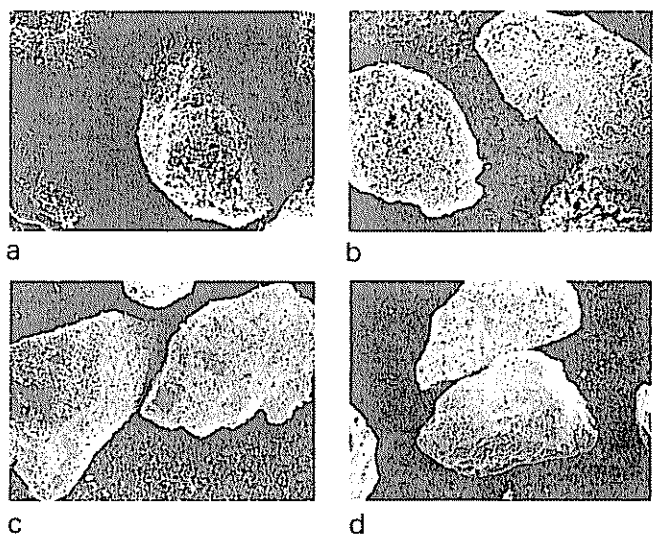

Figure 7 Photomicrographs (150X) of $FeS_{1.14}$ reduced in hydrogen. Sonora pyrite (210–250 μm). (a) 400°C; (b) 450°C; (c) 500°C; (d) 600°C

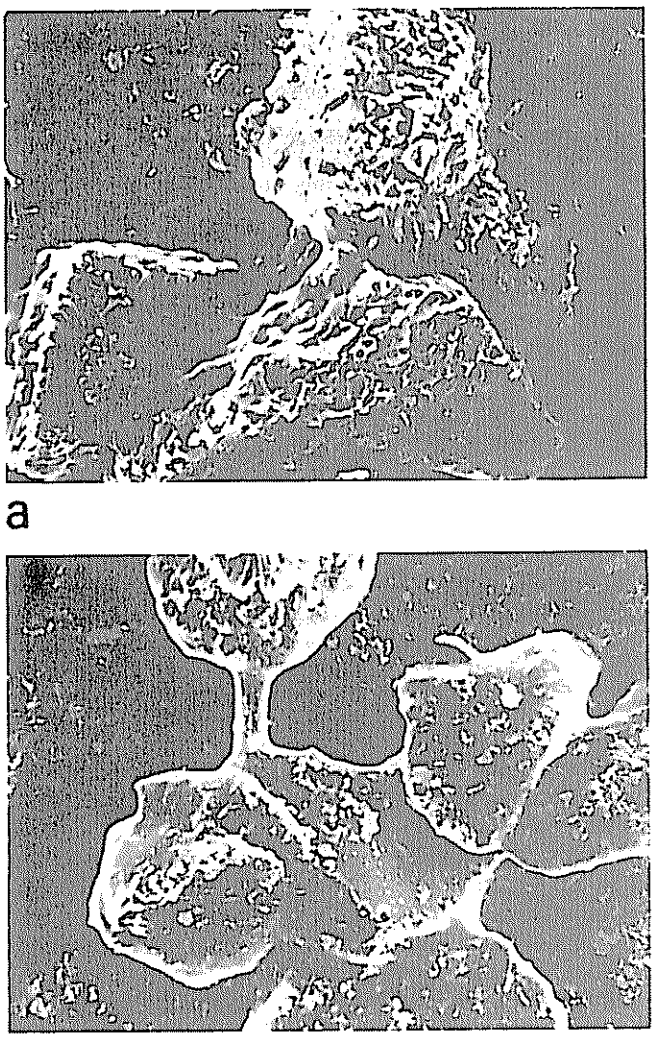

Figure 8 Photomicrographs of $FeS_{1.15}$ reduced in hydrogen at 600°C. Sonora pyrite (44–53 μm). (a) 580x; (b) 406x

shown in *Figure 5*, also decrease with increasing reduction temperature.

Since there appears to be no change in the overall particle size, one must conclude that the solid undergoes a reduction in molar volume during the transformation of pyrite to pyrrhotite to account for the development of porosity. The molar volumes of pyrite and troilite, calculated from X-ray data, are 23.93 and 18.20 cm^3 mol^{-1}, respectively[13]. Thus, in the absence of sintering and retention of original particle volume, the transformation of FeS_2 to FeS should produce a porosity of 23.9% based on the change in molar volume associated with the pyrite–pyrrhotite transition.

At higher temperatures, the decrease in surface area is probably due to sintering, which is associated with increased surface diffusion at the Tammann temperature. Although the pyrrhotites melt over a range of temperature, a melting point of 1150°C is assumed which gives a Tammann temperature of 439°C. From *Figure 5*, above 450°C, the increase in specific surface area is nearly linear with extent of reduction. At a temperature of 400°C, below the Tammann temperature, the increase in specific surface area is much more rapid with extent of conversion. The effects of sintering, using the smaller pyrite particles (44–53 μm) reduced at 600°C, are examined by scanning electron microscopy (*Figure 8*). This shows the extent of intra- and interparticle interaction occurring during the pyrite–pyrrhotite transition.

Two additional pyrite samples were investigated. One sample from Colorado (Rico) was ground to −200 mesh (<74 μm). The other sample was obtained from North Carolina (courtesy of Professor H. Barnes, Pennsylvania State University, labelled NC), and was ground to 210–250 μm. The specific surface areas of these pyrites, measured by krypton adsorption, were 0.098 and 0.0095 $m^2 g^{-1}$, respectively. From the BET plots one can obtain an intercept and the volume of krypton adsorbed in a monolayer. The reciprocal of the product of these two values is equal to a constant, C, which is related to the heat of adsorption of krypton on the adsorbent according to the following equation[15]:

$$C = \exp(E - E_l)/RT \quad (1)$$

where: E = heat of adsorption

E_l = heat of liquefaction of krypton (2020 cal mol^{-1})

R = gas constant

T = temperature (K)

The heats of adsorption of krypton on the various pyrites were significantly different. The values do not correlate with the specific surface areas; however, it is well known that different crystallographic faces may give different heats of adsorption. An investigation was conducted to determine whether an increased area of a particular face existed for different pyrite samples and if these differences could be correlated with the measured heats of adsorption. The pyrite preferentially cleaves along (100) planes[12]. The extent of this preferential cleavage was determined by measuring the amount of preferred orientation using X-ray analysis of pyrite samples allowed to settle in a viscous solution (collodion in amyl acetate) while undergoing vibration in a sonic cleaner. The intensity ratio, I_{200}/I_{311}, is a measure of the relative amount of (100) faces present since the (311) reflection is the major peak obtained with random particle orientation. These data, as well as the values of C and the calculated heats of adsorption, are given in *Table 2*. These data show the expected increase in the I_{200}/I_{311} ratio for the Sonora pyrite upon grinding to a smaller particle size. This determination of preferential cleavage is further supported by the previously determined decrease in R_f upon grinding. The excellent correlation between the heats of adsorption and the relative increase in the (100) faces is given in *Figure 9*.

In-situ observations of the pyrite to pyrrhotite transformations have been made under three different experimental conditions: (1) under constant hydrogen pressure with increasing temperature; (2) under nitrogen pressure with increasing temperature, then changing to a hydrogen pressure at constant temperature; and (3) under vacuum

Table 2 Surface analyses of various pyrites

Pyrite	Particle size (μm)	C	E (cal mol^{-1})	I_{200}/I_{311}
Sonora	210 x 250	11	2390	1.26
Sonora	44 x 53	20	2480	2.60
Rico	<74	42	2590	3.68
NC	210 x 250	11 170	3450	14.1

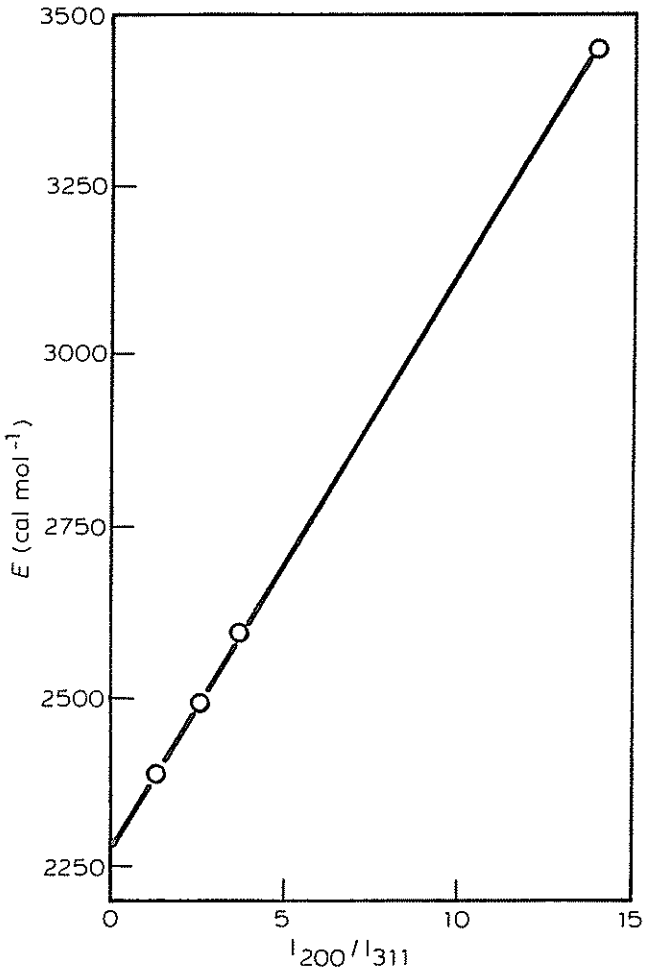

Figure 9 Heat of adsorption of Kr on pyrites as a function of increasing {100} faces

Table 3 In-situ observations of pyrite decomposition

Pyrite sample: (NC) 210–250 μm pyrite crystals
Conditions: 1.48 MPa (200 psig) hydrogen, flow rate 2 cm^3 min^{-1}, heating rate 15°C min^{-1}, magnification 240x.

Figure 10	Temperature (°C)	Observations
(a)	18	Pyrite grain with a highly reflective surface that contains some striations
(b)	445	Granular textured surface replacing highly reflective surface with the striations nearly eliminated

Conditions: 0.687 MPa (85 psig) nitrogen, flow rate 1 cm^3 min^{-1}, heating rate 15°C min^{-1} to a constant temperature 418°C for 30 min in nitrogen, replaced with 4.24 MPa (600 psig) hydrogen, flow rate 2 cm^3 min^{-1}, at a constant temperature 418°C

Figure 11	Temperature (°C)	Observations
(a)	130	Individual pyrite grain, highly reflective with numerous striations
(b)	418	Pyrite grain, after 30 min at temperature in nitrogen, exhibiting some thermal decomposition
(c)	418	Pyrite grain, after 2 min at temperature in 4.24 MPa hydrogen, exhibiting very rapid decomposition
(d)	418	Pyrite grain, after 7 min at temperature in 4.24 MPa hydrogen, exhibiting essentially complete surface decomposition

Pyrite sample: (Sonora) 210–250 μm pyrite crystals
Conditions: 4.8 kPa (–14.0 psig) after nitrogen purge at room temperature, heating rate 10°C min^{-1}.

Figure 12	Temperature (°C)	Observations
(a)	18	Pyrite grain with fair surface reflectivity
(b)	500	Pyrite grain exhibiting slight amount of thermal decomposition near grain centre
(c)	535	Pyrite grain exhibiting increased thermal decomposition product near grain centre
(d)	540	Pyrite grain exhibiting an essentially completely thermally decomposed surface
(e)	550	A different pyrite grain exhibiting fissures developed in final stages of decomposition

conditions with increasing temperature. Typical observations under the three types of experimental conditions are given in *Table 3*.

The observations of pyrite decomposition upon heating to >400°C, under 1.48 MPa (200 psig) hydrogen, are shown in *Figures 10a* and *10b*. At room temperature, the pyrite grain has a highly reflective surface. Upon heating to 445°C, a granular surface texture is developed which is associated with the hydrogen-assisted thermal reduction of the pyrite to pyrrhotite. The pyrrhotite appears as a polycrystalline product on the surface while retaining the original boundaries of the pyrite particle.

A comparative study of the surface alteration, due to the difference in the rate of the pyrite–pyrrhotite transformation, under nitrogen and hydrogen are shown in *Figures 11a–11d*. The pyrite particle, under nitrogen at low temperatures, exhibit highly reflective surfaces. After 30 min in nitrogen at 418°C, the pyrite surface exhibits some thermal decomposition as shown by alteration products forming on the surface, especially within the striations on the surface. In comparison, continued transformation of pyrite to pyrrhotite by the introduction of 4.24 MPa (600 psig) hydrogen pressure in place of the nitrogen shows the same pyrite particle to transform more rapidly in a hydrogen environment. The pyrite decomposition (shown in *Figure 11c*) after only 2 min in hydrogen (4.24 MPa) is much more rapid at the same temperature (418°C) as shown by the increased concentration of the alteration product on the surface, presumably pyrrhotite. Further reduction of the pyrite (*Figure 11d*), after 7 min at the same temperature and pressure shows complete alteration of the surface to a polycrystalline pyrrhotite. These observations are in agreement with the relatively faster reaction rate of pyrite decomposing, under hydrogen, to pyrrhotite and hydrogen sulphide in comparison to the thermal reduction of pyrite, in nitrogen, to pyrrhotite and a polymeric sulphur species[14].

Observations of the alteration of pyrite at near vacuum conditions of 4.8 kPa after initial purging with nitrogen,

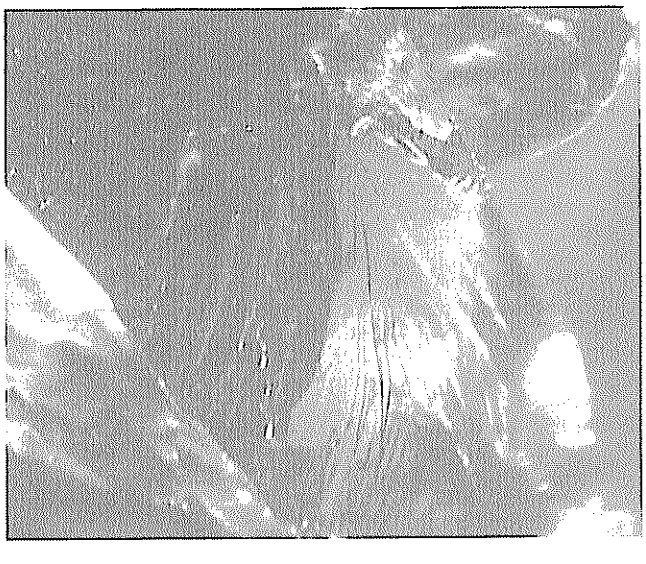

a

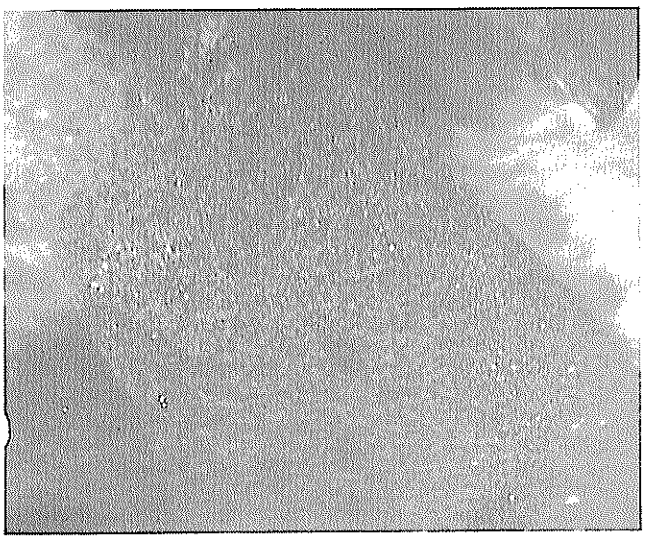

b

Figure 10 Pyrite decomposition to pyrrhotite (240X). NC pyrite (210–250 μm). (a) 18°C, 1.48 MPa hydrogen; (b) 445°C, 1.48 MPa hydrogen

show very little thermal alteration of the pyrite at temperatures <400°C. Although some pyrite particles showed some alteration between 400 and 500°C, the pyrite particle selected for observation (*Figures 12a–12e*) exhibited a slight amount of thermal decomposition near its centre portion at 500°C. The same pyrite particle, after reaching a temperature of 540°C exhibited a completely thermally altered surface. A different pyrite grain (*Figure 12e*) developed fissures in the final stages of decomposition. These observations are in agreement with the slower rate of reduction of pyrite *in vacuo* in comparison to pyrite reduction rates at comparable temperatures under high pressures of hydrogen[14].

CONCLUSIONS

Hydrogen-assisted pyrite reduction, without the presence of hydrocarbons, results in the development of porosity and increased surface area. The specific surface area of Sonora pyrite, between 400 and 600°C, increases with

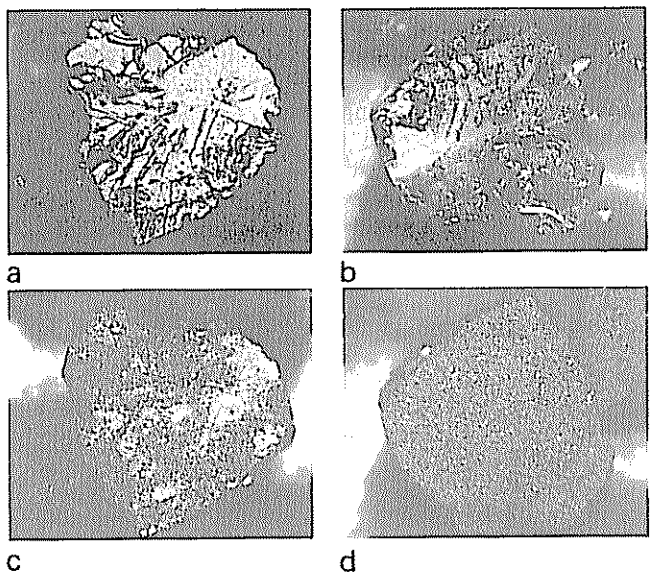

a b c d

Figure 11 *In-situ* reduction of pyrite to pyrrhotite (240x). NC pyrite (210–250 μm). (a) 130°C, 0.687 MPa nitrogen; (b) 418°C, 0.687 MPa nitrogen for 30 min; (c) 418°C, 4.24 MPa hydrogen for 2 min; (d) 418°C, 4.24 MPa hydrogen for 7 min

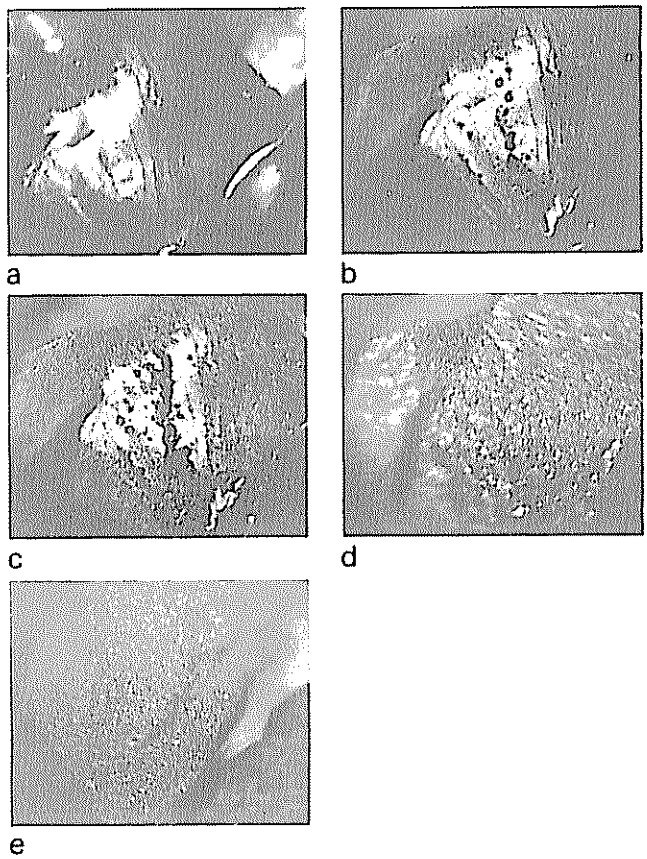

a b c d e

Figure 12 Pyrite–pyrrhotite transformation in vacuum. Sonora pyrite (210–250 μm). (a) 18°C, 4.8 kPa; (b) 500°C, 4.8 kPa; (c) 535°C, 4.8 kPa; (d) 540°C, 4.8 kPa; (e) 550°C, 4.8 kPa (240x)

pyrite conversion. This increase was found to be as much as 10-fold at lower temperatures. Specific surface areas are found to be inversely proportional to reduction temperature with sintering occurring above the Tammann temperature. Explain heats of adsorption on pyrite are found to correlate with the relative increase of (100) faces generated upon grinding.

Direct *in-situ* observations of the pyrite to pyrrhotite transformations have been made at elevated temperatures, under nitrogen and hydrogen pressures, and near vacuum conditions, using newly developed pressure-temperature microscopy. These observations show that the rate of surface decomposition due to the pyrite–pyrrhotite transition is much faster under hydrogen-assisted conditions than under nitrogen or evacuated conditions.

ACKNOWLEDGEMENTS

Support of J. M. Lambert, Jr. by a Mining and Mineral Resources Research Institute Fellowship from the US Department of the Interior is gratefully acknowledged.

REFERENCES

1 Jackson, W. R., Larkins, F. P., Matshall, M., Rash, D. and White, N. *Fuel* 1979, **58**, 261
2 Granoff, B. and Baca, P. M. Sandia Laboratories Energy Report SAND-79-0505, April 1979
3 Morooka, S. and Hamrin, C. E., Jr. *Chem. Eng. Sci.* 1977, **32**, 125
4 Wright, C. H. and Severson, D. E. *Am. Chem. Soc., Div. Fuel Chem., Preprints* 1972, **16**(2), 68
5 Lambert, J. M., Jr. *Fuel* 1982, **61**, 777
6 Guin, J. A., Lee, J. M., Fan, C. W., Curtis, C. W., Lloyd, J. L. and Tarrer, A. R. *Ind. Eng. Chem. Process Des. Dev.* 1980, **19**, 440
7 Brunauer, S., Emmett, P. H. and Teller, E. *J. Am. Chem. Soc.* 1938, **60**, 309
8 Rosenberg, A. J. *J. Am. Chem. Soc.* 1956, **78**, 2929
9 Thomas, J. M. and Thomas, W. J. 'Introduction to the Principles of Heterogeneous Catalysis', Academic Press, New York, 1967, 85
10 Yund, R. A. and Hall, H. T. *Econ. Geol.* 1969, **64**, 420
11 Lambert, J. M., Jr., Simkovich, G. and Walker, P. L., Jr. *Fuel* 1980, **59**, 687
12 Frenzel, G. and Bloss, F. D. *Am. Mineral.* 1967, **49**, 1350
13 'Handbook of Chemistry and Physics', (Ed. R. C. Weast), 57th Ed., CRC Press, Boca Raton, Florida, 1976–77
14 Lambert, J. M., Jr. *Ph.D. Thesis* Fuel Science Section, Department of Material Science and Engineering, Pennsylvania State University, May 1982
15 Thomas, J. M. and Thomas, W. J. 'Introduction to the Principles of Heterogeneous Catalysis', Academic Press, New York, 1967, 47